Article

Dense Molecular Environments of B[e] Supergiants and Yellow Hypergiants

Michaela Kraus [1,*] , **Michalis Kourniotis** [1] , **María Laura Arias** [2,3] , **Andrea F. Torres** [2,3] and **Dieter H. Nickeler** [1]

1   Astronomical Institute, Czech Academy of Sciences, Fričova 298, 251 65 Ondřejov, Czech Republic
2   Departamento de Espectroscopía, Facultad de Ciencias Astronómicas y Geofísicas,
     Universidad Nacional de La Plata, Paseo del Bosque S/N, La Plata B1900FWA, Argentina
3   Instituto de Astrofísica de La Plata (CCT La Plata-CONICET, UNLP) Paseo del Bosque S/N,
     La Plata B1900FWA, Argentina
*   Correspondence: michaela.kraus@asu.cas.cz

Abstract: Massive stars expel large amounts of mass during their late evolutionary phases. We aim to unveil the physical conditions within the warm molecular environments of B[e] supergiants (B[e]SGs) and yellow hypergiants (YHGs), which are known to be embedded in circumstellar shells and disks. We present *K*-band spectra of two B[e]SGs from the Large Magellanic Cloud and four Galactic YHGs. The CO band emission detected from the B[e]SGs LHA 120-S 12 and LHA 120-S 134 suggests that these stars are surrounded by stable rotating molecular rings. The spectra of the YHGs display a rather diverse appearance. The objects 6 Cas and V509 Cas lack any molecular features. The star [FMR2006] 15 displays blue-shifted CO bands in emission, which might be explained by a possible close to pole-on oriented bipolar outflow. In contrast, HD 179821 shows blue-shifted CO bands in absorption. While the star itself is too hot to form molecules in its outer atmosphere, we propose that it might have experienced a recent outburst. We speculate that we currently can only see the approaching part of the expelled matter because the star itself might still block the receding parts of a (possibly) expanding gas shell.

Keywords: stars: massive; stars: supergiants; stars: winds; outflows; circumstellar matter

1. Introduction

The evolution of massive stars ($M_{ini} \gtrsim 8\,M_\odot$) bears many uncertainties, which render it difficult to trace such objects from the cradle up to their spectacular explosion as supernova. One major hindrance is the poorly constrained mass loss due to stellar winds that the stars experience along the course of their evolution. Furthermore, the post-main sequence evolution of massive stars encounters phases in which the stars lose a significant amount of mass due to episodically enhanced mass loss or occasional mass eruptions, both of poorly understood origin. The ejected mass can accumulate around the star in rings, shells, or bipolar lobes, as seen in some B- or B[e]-type supergiants (e.g., Sher 25 [1,2], MWC 137 [3,4], SBW1 [5]), yellow hypergiants (IRC+10 420 [6] and Hen 3-1379 [7]), many luminous blue variables [8,9], and Wolf-Rayet stars [10–14].

Two groups of evolved massive stars are particularly interesting. These are the B[e] supergiants (B[e]SGs) and the yellow hypergiants (YHGs). Both types of objects have dense and warm circumstellar environments, and representatives of both classes of objects show (at least occasionally) emission from hot molecular gas.

1.1. B[e] Supergiants

The group of B[e]SGs consists of luminous ($\log(L_*/L_\odot) \geq 4.0$) post-main sequence B-type emission line stars. Besides large-scale ejecta (with sizes of several pc) detected in some B[e]SGs [3,9], all objects have intense winds and are surrounded by massive

disks on small scales (up to ~100 AU) [15–17], giving rise to the specific emission features characterizing stars with the B[e] phenomenon [18]. These disks give shelter to a diversity of molecular and dust species, and the near-infrared (NIR) is an ideal wavelength regime to detect molecular emission features that, when resolved with high spectral resolution, provide insight into the physical properties of the disks and reveal the disk dynamics.

The most commonly observed molecule is CO. The emission from its first-overtone bands arises in the *K*-band around 2.3 μm and has been detected in about 50% of the B[e]SGs [19]. Besides the main isotope ^{12}CO, emission from ^{13}CO is seen in considerable amounts [20,21], confirming that the matter from which the disks have formed contains processed material that must have been released from the stellar surface [22].

Emission from the first-overtone bands of SiO, arising in the *L*-band around 4 μm, has been reported for some Galactic B[e]SGs [23]. SiO has a lower binding energy than CO. It thus forms at distances farther away from the star than CO. The individual ro-vibrational lines in both CO and SiO are kinematically broadened with a double-peaked profile, and (quasi-)Keplerian rotation of the molecular gas around the central object has been suggested as the most likely explanation to interpret the spectral appearance [17,23–28].

Observations of B[e]SGs in the NIR are sparse. But persistent CO band emission over years and decades has been detected in numerous objects [21,29,30] and has been used as one of the criteria to identify and classify stars as B[e]SGs in Local Group galaxies [31,32]. However, in a few cases, considerable variability in these emission features has been reported as well. The most striking object is certainly the B[e]SG star LHA 115-S 65 in the Small Magellanic Cloud (SMC), for which a sudden appearance of CO band emission has been recorded [33]. The disk around this object is seen edge-on, and in addition to its rotation around the central object, it also drifts outwards, very slowly and with a velocity decreasing with distance from the star and reaching about zero [34]. This slowdown might have resulted in a build-up of density in regions favorable for molecule condensation and for excitation of the CO bands.

Furthermore, LHA 115-S 18 in the SMC showed no CO band emission back in 1987/1989 [35], whereas follow-up observations in November 1995 taken with a more than three times higher resolution displayed intense CO bands [36], which were also seen in the observations acquired in October 2009 [21].

In the spectrum of the Galactic B[e]SG MWC 349, intense CO band emission appeared in the early 1980s [37]. It was still observable in 2013, but by then the CO gas had clearly cooled and the emission intensity had significantly decreased, which has been interpreted as due to expansion and dilution of the circumstellar disk [38]. Two more objects in the Large Magellanic Cloud (LMC) displayed indications of CO band variability, most likely related to inhomogeneities within the distribution of the molecular gas around the central star. These are LHA 120-S 73 [24] and LHA 120-S 35 [27].

In the optical range, indications for emission from TiO molecular bands have been found in six B[e]SGs [24,27,39,40]. All six objects reside in the Magellanic Clouds, and five of them also have CO band emission[1]. No Galactic B[e]SG has been reported to date to display TiO band emission [19].

1.2. Yellow Hypergiants

With temperatures in the range $T_{eff} \simeq 4000$–8000 K and luminosities $\log(L/L_{\odot})$ spreading from 5.2 to 5.8, the YHGs populate a rather narrow domain in the Hertzprung-Russel (HR) diagram. The stars are in their post-red supergiant (post-RSG) evolutionary phase [41], and their luminosities place them on evolutionary tracks of stars with initial masses in the range $M_{ini} \simeq 20$–$40\,M_{\odot}$. Evolutionary calculations of (rotating) stars in this mass range have shown that these objects can indeed evolve back to the blue, hot side of the HR diagram [42], whereas stars with lower initial mass just reach the RSG stage before they explode as SNe of type II-P. Support for this theoretical scenario is provided by the lack of high-mass ($M_{ini} \geq 18\,M_{\odot}$, i.e., with luminosities $\log L/L_{\odot} > 5.1$) RSG progenitors for this type of supernovae [43,44].

As post-RSGs, the YHGs might be expected to be embedded in envelopes, remnants of the previous mass-losing activities during the RSG stage. However, surprisingly, so far, only about half of the YHGs have been reported to have a dusty and/or cold molecular envelope. These are the Galactic objects IRC +10420 [45–47], HR 5171A [48], HD 179821 [49] and Hen 3-1379 [7,50], three YHGs in the LMC (HD 269953, HD 269723, HD 268757, [51]), as well as Var A [52] and three more YHG candidates in the galaxy M33 [53].

A typical classification characteristic of YHGs is the occurrence of outbursts that can be clearly discriminated from the more regular (cyclic) brightness variability due to stellar pulsations. During such an outburst event, the star inflates, its brightness drastically decreases, and the object seems to undergo a red loop evolution in the HR diagram. Molecules such as TiO and CO can form in the cool, outer atmospheric layers, leading to intense absorption structures in the optical and NIR, respectively, and the object's entire spectral appearance resembles that of a much later spectral type. The outbursts are most likely connected with enhanced mass loss or mass eruptions from the star, which might be connected to non-linear instabilities such as finite-time singularities or blow-ups typically occurring in fluid dynamics [54] or to strange-mode instabilities [55,56] as recent computations propose [57]. The duration of the outbursts can range from months to decades before the star appears back at its real location in the HR diagram.

The bona-fide YHG, ρ Cas, experienced four documented outbursts during the past 80 years with variable duration (from weeks up to three years) and amplitude (0.29 to 1.69 mag), connected with significant changes in its spectral appearance [58–61], whereas Var A in M33 presumably underwent an eruption around 1950 that lasted $\sim$45 years [52]. The object V509 Cas experienced mass-loss events in the seventies, during which the star's apparent temperature decreased significantly. Since then, the star has displayed a steady increase in its effective temperature from $\sim$5000 K in 1973 to $\sim$8000 K in 2001 [62], and since then it has stabilized at that temperature [63]. Furthermore, IRC +10420 changed its spectral type from F8 to mid- to early A, connected with an increase in temperature over a period of about 30 years with an average rate of $\sim$120 K per year [64,65]. The light curves of other YHG candidates also display outburst activity in connection with variable mass loss [51,53]. However, in many cases, the mass-loss episodes appear to be short, so that the released material expands and dilutes without creating detectable large-scale circumstellar envelopes [66].

Nevertheless, many YHGs are surrounded (or were for some period in the past) by hot molecular gas traced by first-overtone CO band emission, suggesting that the objects are embedded in a dense and hot environment. Whether the molecular gas is arranged in a ring revolving around the object, as in the case of the B[e]SGs, is currently not known. However, the CO band spectral features in YHGs seem to be much more variable than in their hotter B[e]SG counterparts, especially because they often appear superimposed on photospheric CO band absorption that forms during the expansion and cooling periods of the long-term pulsation cycles, especially of the cooler YHGs, or during outburst events. One such candidate with cyclic CO band variability is ρ Cas. During its pulsation cycles, CO band emission appears when the star is hottest (maximum brightness) and most compact, whereas CO bands are seen in absorption when the star is coolest (minimum brightness) and most inflated [67]. It has been speculated that the appearance of CO bands in emission might be related to propagating pulsation-driven shock waves in the outer atmosphere of the star [67]. An alternative scenario would also be conceivable, in which the CO emission could be permanent, arising from a circumstellar ring or shell and being detectable only during phases in which no photospheric absorption compensates the emission [60]. Support for the latter scenario is provided by the fact that the CO emission features remain at constant radial velocities (along with other emission lines formed in the circumstellar environment such as [Ca II] and Fe I, [60]) whereas the absorption components change from red- to blue-shifted, in phase with the pulsation cycle.

The object ρ Cas is, to date, the best monitored YHG in the NIR. For many other YHGs observations in the *K*-band have been taken only sporadically. Hence, not much can be

said or concluded about the variability rhythm of their CO band features. Occasional CO band emission has been reported for the galactic objects HD 179821 [68,69], V509 Cas [70], [FMR2006] 15 [71], and the two LMC objects HD 269723 and HD 269953 [21,29]. The latter even displays emission from hot water vapor and is, so far, the only evolved massive star with such emission features from its environment [72].
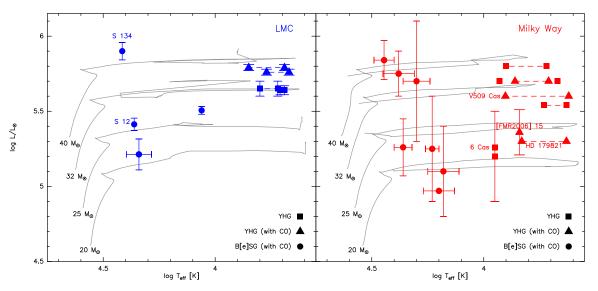
1.3. Motivation and Aims

The appearance of CO band emission in the NIR spectra of B[e]SGs and YHGs suggests that similar physical conditions may prevail in the circumstellar environments of both groups of objects. In depth studies of these conditions are rare though.

For the B[e]SGs in the Magellanic Clouds CO, column densities, temperatures, and $^{12}CO/^{13}CO$ isotopic ratios were determined based on medium-resolution *K*-band spectra [21]. The resolution of these spectra was, however, too low to derive the gas kinematics with high confidence. On the other hand, high-resolution *K*-band spectra of the Galactic B[e]SG sample allowed to obtain the CO dynamics [17,73], whereas in most cases the spectral coverage was too short to infer about the density and temperature of their hot molecular environment.

The situation for the YHGs is even worse. Besides for ρ Cas [67] and for the LMC object HD 269953 [21,72] no attempts have been undertaken so far to study their warm molecular environments in more detail and to derive the parameters of the CO band emitting regions.

Therefore, we started to systematically observe both the B[e]SGs and the YHGs in the Milky Way and Magellanic Clouds to fill this knowledge gap. A further motivation for our research is provided by the location of the B[e]SGs with CO band emission in the HR diagram. As has been mentioned previously for the Magellanic Clouds sample [19], these objects cluster around luminosity values $\log L/L_\odot \simeq 5.0$–5.9, whereas B[e]SGs that are more luminous than ~5.9 or less luminous than ~5.0 do not show CO band emission. The same holds when inspecting the Galactic B[e]SGs. In the left panel of Figure 1 we depict the LMC objects, whereas in the right panel we display the Galactic sample[2] from [17,38]. The YHGs in the LMC [51] and the Milky Way [75] have been added to the plots[3]. Their positions with maximum and minimum effective temperature values, as reported in the literature, have been connected with dashed lines. Errors in temperature and luminosity are indicated when provided by the corresponding studies.

Interestingly, the YHGs and the B[e]SGs with CO band emission share similar evolutionary tracks, which is particularly evident for the Galactic objects. This raises the question of whether evolved stars in this particular mass range suffer from specific instabilities in the blue and yellow temperature regimes independent of their evolutionary state. Such instabilities need to have the potential to drive mass ejections or eruptions, and the released mass would have to be dense and cool enough to create the required conditions for the formation of significant amounts of molecules generating intense band emission.

Figure 1. HR diagram with evolutionary tracks for LMC ($Z = 0.006$, [76], left panel) and solar ($Z = 0.014$, [42], right panel) metallicity for models of rotating stars ($v/v_{\mathrm{crit}} = 0.4$) with initial masses from 20–40 $M_{\odot}$. Shown are the positions of LMC (blue symbols) and Galactic (red symbols) objects. Only B[e]SGs with hot circumstellar molecular CO gas are shown. These populate similar evolutionary tracks as the YHGs. The minimum and maximum temperature values (where known) of the YHGs are connected by dashed lines. YHGs with reported (at least once) CO band emission are shown with triangles. The stars of the current study are labeled.

1.4. Selection of Targets

For our current study, we have selected two B[e]SGs from the LMC. These are the objects LHA 120-S 12 and LHA 120-S 134. Both are known to display CO band emission (see, e.g., [21]), but both of them lack high-resolution *K*-band spectra to derive the CO kinematics. Furthermore, we have selected four Galactic YHGs, [FMR2006] 15, HD 179821, V509 Cas, and 6 Cas. Of these, only the former three objects were reported in the literature to display (at some epochs) CO band emission. The basic stellar parameters of all objects, as obtained from the literature, are listed in Table 1.

Table 1. Stellar parameters. Errors are given where available.

Object	*G* [mag]	K_s [mag]	log T_{eff} [K]	log $L/L_{\odot}$	Ref.	*d* [kpc]	Ref.
LHA 120-S 12	12.4	10.2	4.36	5.34 ± 0.04	[15]	49.6 ± 0.5	[77]
LHA 120-S 134	11.4	8.6	4.41	5.90 ± 0.06	[15]	49.6 ± 0.5	[77]
[FMR2006] 15	19.5	6.7	3.84	5.36 ± 0.15	[71]	6.6 ± 0.9	[71]
6 Cas	—	3.4	3.93	5.13	[78]	2.8 ± 0.3	[79]
V509 Cas	5.0	1.7	3.90	5.60	[63,80]	1.4 ± 0.5	[62] [a]
HD 179821	7.5	4.7	3.83	5.30	[75,81]	5.3 ± 0.3	[81,82]

Note: The *G* and K_s-band magnitudes are from *GAIA* Early Data Release 3 [82] and from the 2MASS point source catalog [83], respectively. The YHG effective temperatures refer to the hot state. No *GAIA G*-band measurement is available for 6 Cas. [a] Listed distance is based on the *HIPPARCOS* parallax of 0.73 ± 0.25. The new *GAIA* Early Data Release 3 parallax of 0.2507 ± 0.0633 [82] places the object at a distance of ∼4 kpc.

2. Observations and Data Reduction

High-resolution spectra ($R \sim 50{,}000$) of the two B[e]SGs were acquired with the visitor spectrograph Phoenix [84] mounted at GEMINI-South. The spectra were taken on 20 December 2004 and 30 November 2017 under program IDs GS-2004B-Q-54 and GS-2017B-Q-32. The observations were carried out in the *K*-band with two different filters,

K4396 and K4308. The central wavelength was chosen such that the wavelength ranges cover the first and second band heads of the first-overtone CO band emission.

Medium-resolution *K*-band spectra of the YHGs have been acquired with the Gemini Near-InfraRed Spectrograph (GNIRS, [85,86]) at GEMINI-North under Program IDs GN-2019A-Q-204, GN-2019B-Q-418, and GN-2021A-Q-315.

The spectrum of [FMR2006] 15 was observed on 12 May 2019 centered on $\lambda = 2.35\,\mu$m. The instrument configuration was a short camera (0.15″ per pixel) with the 0.3″ slit and the 111 l mm^{-1} grating, resulting in a resolving power of $R \sim 5900$.

V509 Cas and 6 Cas were observed on 21 December 2019 with the instrumental configuration: Long camera (0.05″ per pixel) with the 0.10″ slit and the 321 mm^{-1} grating which provides a resolving power of $R \sim 5100$. The observations were centered on $\lambda = 2.35\,\mu$m.

HD 179821 was observed on 7 April 2021 with two different central wavelengths $\lambda = 2.14\,\mu$m and 2.33 μm and with the following instrument configuration: a short camera (0.15″ per pixel), the 0.3″ slit, and the 111 l mm^{-1} grating, resulting in a resolving power of $R \sim 5900$.

For all objects, a telluric standard star (usually a late B-type main sequence star) was observed close in time and airmass. For optimal sky subtraction, the star was positioned at two different locations along the slit (A and B), and the observations were carried out in ABBA cycles. Data reduction and telluric correction were performed using standard IRAF[4] tasks. The reduction steps consist of subtraction of AB pairs, flat-fielding, wavelength calibration (using the telluric lines), and telluric correction. The observing log is given in Table 2, where we list the star name, object class, observing date (UT), used instrument, covered wavelength range, spectral resolution *R*, and resulting signal-to-noise ratio (SNR).
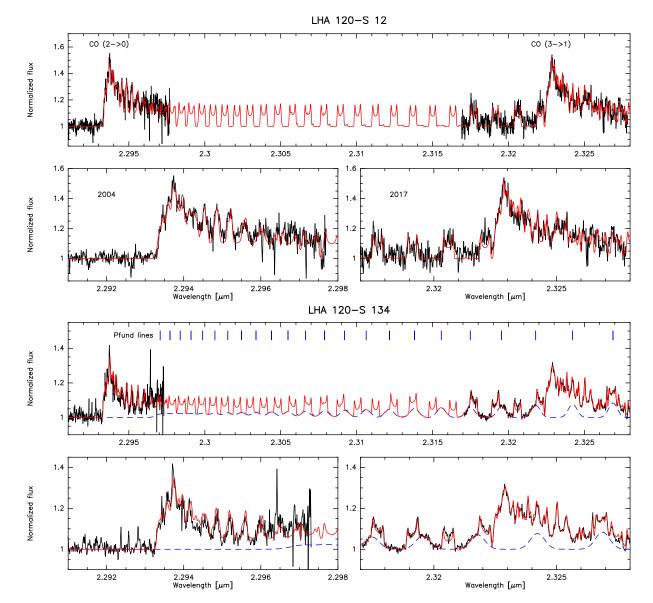
Table 2. Observation log.

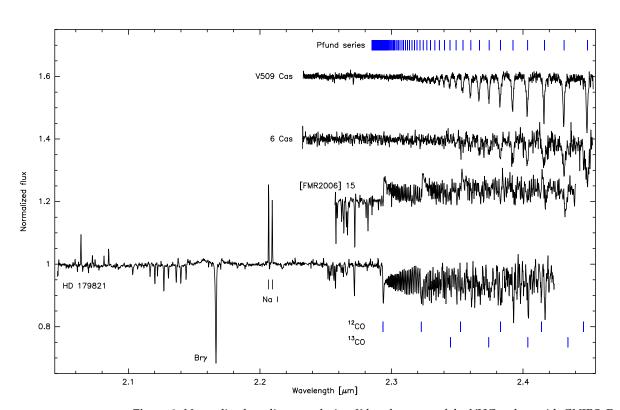| Object	Class	Obs Date [yyyy-mm-dd]	Instrument	λ_{min}–λ_{max} [μm]	R	SNR
LHA 120-S 12	B[e]SG	2004-12-20	Phoenix	2.291–2.300	50,000	35
		2017-11-30	Phoenix	2.319–2.330	50,000	20
LHA 120-S 134	B[e]SG	2017-11-30	Phoenix	2.290–2.299	50,000	40
		2017-11-30	Phoenix	2.319–2.330	50,000	100
[FMR2006] 15	YHG	2019-05-12	GNIRS	2.257–2.440	5900	300
6 Cas	YHG	2019-12-21	GNIRS	2.232–2.453	5100	100
V509 Cas	YHG	2019-12-21	GNIRS	2.233–2.453	5100	140
HD 179821	YHG	2021-04-07	GNIRS	2.046–2.424	5900	250

3. Results

3.1. Description of the Spectra

CO band head emission is detected in both B[e]SGs (black lines in Figure 2) despite the low quality of some of the spectral pieces and some telluric remnants in the red parts of the short wavelength portions (left lower panels). The spectrum of LHA 120-S 134 contains additional emission lines from the hydrogen Pfund series. Intense emission in these recombination lines has already been reported from that star based on medium-resolution spectra [21]. No contribution from the Pfund lines is seen in the spectra of LHA 120-S 12.

Figure 2. Best fitting model (red) to the normalized Phoenix spectra (black) of LHA 120-S 12 (**top**) and LHA 120-S 134 (**bottom**). For each star we display the entire fit to the total spectrum (top panels) and the zoom to the band heads (bottom panels). Emission from the Pfund series (blue dashed line), detected in the spectrum of LHA 120-S 134, is included in the total fit.

The *K*-band spectra of the YHGs display a diverse appearance, as depicted in Figure 3. Two stars possess just Pfund lines in absorption (V509 Cas and 6 Cas) and an otherwise featureless spectrum, in agreement with their high effective temperature ($T_{\text{eff}} \geq 8000\,$K, see Table 1). The star [FMR2006] 15 shows CO band emission overimposed on the atmospheric spectrum of a presumably late-type star. In HD 179821 the CO bands and the Br γ line are in absorption along with numerous other photospheric lines, whereas the Na I $\lambda\lambda 2.206, 2.209$ doublet shows prominent emission.

Figure 3. Normalized medium-resolution *K*-band spectra of the YHGs taken with GNIRS. For better visualization, the spectra have been offset along the flux axis. Positions of the CO band heads and of the lines from the Pfund series are marked by ticks. The lines of Brγ and of the Na I doublet are labeled as well.

3.2. Modeling of the CO Band and Pfund Line Emission

We model the CO emission using our molecular disk code [87] that has been developed to compute the ro-vibrational bands from a rotating ring (or disk) of circumstellar gas under local thermodynamic equilibrium conditions. The calculations are carried out for the two main isotopes, ^{12}CO and ^{13}CO [21,22].

The high-resolution spectra of the two B[e]SGs display kinematic broadening of the individual ro-vibrational lines in the form of a double-peaked profile (Figure 2). Such a profile can be interpreted either as rotation around the central object or as an equatorial outflow. Since B[e]SGs are known to be surrounded by (quasi-)Keplerian rotating disks, the assumption of rotation as the most likely broadening mechanism seems to be justified. The situation for the YHG star [FMR2006] 15 is less clear. The medium-resolution spectrum provides no clear hint about a possible double-peaked shape of the individual lines. Therefore, we can only derive an upper limit for a possible rotational (or outflow) contribution to the total dynamics.

Due to the high sensitivity of the CO band intensity to the gas temperature and column density, the observed emission traces the hottest and densest molecular regions. Therefore, it is usually sufficient to consider a single ring of gas with constant density and temperature, reducing the number of free parameters to the column density N_{CO}, temperature T_{CO}, the isotope ratio ^{12}CO/^{13}CO, and the gas kinematics split into contributions of the rotation velocity projected to the line of sight $v_{rot,los}$, and of a combined thermal and turbulent velocity in the form of a Gaussian component v_{Gauss}.

The best-fitting CO parameters obtained for the three objects are listed in Table 3, and the total emission spectra are included (in red) in Figure 2 for the two B[e]SGs. It is noteworthy that the two CO band heads of LHA 120-S 12 can be reproduced fairly well with the same model parameters, despite the fact that the spectral pieces have been observed 13 years apart. This implies that the ring of CO gas around LHA 120-S 12 is stable on longer timescales.
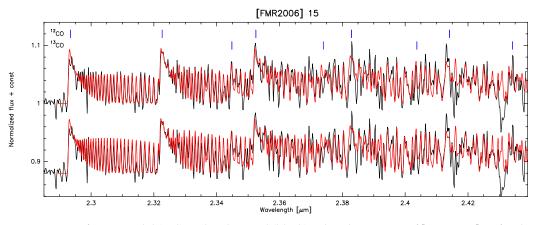
Table 3. Best fitting CO parameters.

Object	T_{CO} [K]	N_{CO} [$\times 10^{21}$ cm^{-2}]	$v_{rot,los}$ [km s^{-1}]	v_{Gauss} [km s^{-1}]	^{12}CO/^{13}CO
LHA 120-S 12	2800 ± 200	1.5 ± 0.2	27 ± 2	3 ± 1	20 ± 2
LHA 120-S 134	2300 ± 100	2.0 ± 0.1	30 ± 1	1.5 ± 0.5	15 ± 2
[FMR2006] 15	3000 ± 200	2.0 ± 0.2	20 ± 5	15 ± 5	4 ± 2
[FMR2006] 15	3000 ± 200	2.0 ± 0.2	0	20 ± 5	4 ± 2

Note: The ^{12}CO/^{13}CO values for LHA 120-S 12 and LHA 120-S 134 have been derived by [20,21], respectively. Our Phoenix spectra do not reach the wavelength region of the ^{13}CO bands.

The spectrum of LHA 120-S 134 displays emission from the hydrogen Pfund line series superimposed on the CO band spectrum[5]. These Pfund lines appear to be broad with no indication of a double-peaked profile shape. To include the contribution of these lines to the total emission spectrum, we apply our code developed for the computation of the hydrogen series according to Menzel case B recombination, assuming that the lines are optically thin [87]. We fix the electron temperature at 10,000 K, which is a reasonable value for ionized gas around an OB supergiant star and, using a Gaussian profile, we obtain a velocity of 53 ± 3 km s^{-1}. Similar velocity values for the lines from the Pfund series have been found for various B[e]SGs (see [20,21,26]). These rather low values compared with the wind velocities of classical B supergiants might suggest that the Pfund lines form in a wind emanating from the surface of the ionized part of the circumstellar disk. The electron density can be derived from the maximum number of the Pfund series visible in the spectrum. For LHA 120-S 134, this number corresponds to the line Pf(57), resulting in an electron density of $(5.8 \pm 0.5) \times 10^{12}$ cm^{-3} within the Pfund line forming region. Having the parameters for the Pfund emission fixed, we compute the contribution of the Pfund series to the total emission spectrum of LHA 120-S 134. This contribution is shown in blue in Figure 2.

The best-fitting CO model for the YHG [FMR2006] 15 is depicted in Figure 4 (top). It should be noted that the contribution of the rotation (respectively outflow) component should be considered an upper limit. A double-peaked profile corresponding to such a velocity might be hidden within the CO band structure. Only high-resolution observations will tell whether such a profile component is really included. We found that a model omitting this velocity component and using instead just a single Gaussian profile (added to Table 3) results in a similar but slightly less satisfactory fit because the intensity of many individual ro-vibrational lines is overestimated in the short wavelength domain (Figure 4, bottom).

Figure 4. Best fitting model (red) to the observed (black) *K*-band spectrum of [FMR2006] 15 for the model including a rotational component (**top**) and a pure Gaussian broadening (**bottom**).

　　　The rotation velocity of the CO gas allows us to estimate the distances of the CO-emitting rings from the central object. For this, we need to know the current stellar masses. Considering the stellar effective temperatures, luminosities (from Table 1), and the carbon isotope ratios (from Table 3), we search for the best matching evolutionary models for each of our targets utilizing the stellar evolution track interpolation tool SYCLIST[6]. To reproduce the observed carbon isotope ratios, we vary the initial stellar rotation rate between zero and the maximum offered value of 0.4 and select those evolutionary tracks that fit both the stellar location in the HRD and the carbon isotope ratio. The metallicities used are 0.006 for the LMC objects and 0.014 for the Galactic star. Table 4 lists the stellar radii of our targets along with the most likely initial masses, initial rotation rate, and the resulting current masses. We note that according to these evolutionary tracks, the B[e]SGs seem to have evolved just off the main sequence, whereas the low carbon isotope ratio measured in [FMR2006] 15 clearly places this object on the post-RSG path. For the reason that no proper values for the disk inclination angles are known, we provide the distances of the CO-emitting rings as a function of the inclination angle. These are lower limits to the real distances. We refrain from adding a distance of the CO emitting region for [FMR2006] 15 because of the speculative nature of its rotation component.

Table 4. Estimated current stellar masses and distances of the CO emitting rings from the star.

Object	R_* [$R_\odot$]	M_{in} [$M_\odot$]	v/v_{crit} [km s^{-1}]	M_* [$M_\odot$]	$r_{CO}/(\sin i)^2$ [cm]	$r_{CO}/(\sin i)^2$ [R_*]
LHA 120-S 12	30	26	0.25	25	4.6×10^{14}	218.0
LHA 120-S 134	44	45	0.36	40	5.9×10^{14}	192.7
[FMR2006] 15	333	25	0.40	13	—	—

4. Discussion

　　　We have detected CO band emission in three objects and CO band absorption in one object in our sample. To assess a possible CO variability, we summarize in Table 5 information about previous detections of CO band features in the *K*-band from the literature, including our results.

　　　The number of observations in the *K*-band over the last 3–4 decades is sparse for all objects, but the two B[e]SGs continuously display emission over a time interval of 32 years. The diversity in spectral resolution used for the observations makes it difficult to compare the shape and intensity of the emission bands and, hence, to judge variability. Only for LHA 120-S 12, we can say that no significant variability seems to have taken place between our observations acquired in 2004 and in 2017.

　　　For the YHGs, the situation is different. Three of them clearly show variability in their CO bands, ranging from emission over complete disappearance to absorption (or a combination of emission and absorption). The changes are on time scales ranging from months to years. The exception is 6 Cas, which has not been reported previously to have CO bands, and our own observations taken 25 years later also lack any CO band features.

　　　In the following, we briefly describe the known characteristics of each of our targets with respect to stellar variability and the properties of the circumstellar environments in order to incorporate our new observational results.

Table 5. CO band detection in the *K*-band and CO variability.

Object	Obs Date	*R*	CO Bands	Ref.
LHA 120-S 12	1985-12-28	450	em	[29]
	2004-12-17	50,000	em	TW
	2009-10-14	4500	em	[20,21]
	2017-11-30	50,000	em	TW
LHA 120-S 134	1985-12-29	450	em	[29]
	2009-11-10	4500	em	[21]
	2017-11-30	50,000	em	TW
[FMR2006] 15	2005-09-15	1000	weak abs	[88]
	2006-05-05	17,000	em	[71]
	2006-08-12	17,000	none	[71]
	2019-05-12	5900	em	TW
6 Cas	1996-08-31	1800	none	[89]
	2019-12-21	5100	none	TW
V509 Cas	1979-1980	32,000	em + abs (variable)	[70]
	1988	N.A.	none	[67]
	2003-11-20	300	none	[67]
	2004-10-30	300	none	[67]
	2019-12-21	5100	none	TW
HD 179821	1989-07-14	1600	em	[69]
	1990-09-26	760	em	[68]
	1991-11-04	330	em	[68]
	1992 August	N.A.	none	[69]
	1997-04-19	1800	none	[89]
	2000-10-18	N.A.	none	[67]
	2021-04-07	5900	abs	TW

Note: em = emission; abs = absorption; TW = this work; N.A. = no information available.

LHA 120-S 12 (=SK −67 23)

The object LHA 120-S 12 was first mentioned in the catalog of Hα-emission stars in the Magellanic Clouds [90]. Follow-up observations recorded an intense IR excess due to hot dust [91]. The two-component wind associated with the star led to its classification as B[e]SG [15], and the high degree of intrinsic polarization suggested a high, but not fully edge-on, viewing angle towards the object and its dusty disk [92]. Shell-line profiles were seen in the NIR, consistent with the high inclination angle of the system [21]. Observations with the *Spitzer Space Telescope* revealed silicate dust within the circumstellar disk, based on weak features in the star's mid-IR spectrum, but no IR nebulosity has been detected in association with the object [93].

The first detection of CO band emission from LHA 120-S 12 was in 1985 based on a low-resolution *K*-band spectrum [29]. This spectrum clearly depicted four first-overtone band heads, similar to the observations collected in 2009. Modeling of the latter [20] resulted in similar parameters for the CO temperature and column density to those we found from the high-resolution spectra taken before (2004) and afterwards (2017). Moreover, we see no changes in the rotation velocity, projected to the line of sight, within the time span of 13 years between our two observations. Therefore, we believe that the CO-emitting ring revolving around LHA 120-S 12 is rather stable, with no detectable outflow or inflow.

A similar (projected) rotation velocity to that for CO can be inferred from the double-peaked profiles of the [CaII] lines resolved in high-resolution optical spectra of LHA 120-S 12 [94], although a Gaussian component with a higher value might be necessary to smooth out the sharp synthetic double-peaked rotation profile in order to reproduce the shape of the observed forbidden lines.

LHA 120-S 134 (=HD 38489, SK −69 259, MWC 126)

The object LHA 120-S 134 was listed in the catalog of B and A-type stars with bright hydrogen lines published in 1933 [95] under the Mount Wilson Catalogue (MWC) number 126 with classification as Beq. Its hybrid spectra with narrow (equivalent widths of 30–50 km s^{-1}) emission lines of neutral and low-ionized metals in the optical spectral range [15] and very broad P Cygni profiles (implying a wind terminal velocity of ∼2300 km s^{-1}) of high-ionized metals in the ultraviolet [96], along with the detected intense IR excess emission characteristic of hot circumstellar dust [91], resulted in the classification of the star as B[e]SG. A small inclination angle has been proposed for LHA 120-S 134 [15], and the relatively low measured degree of polarization supports a close to pole-on orientation of the star plus disk system [92].

LHA 120-S 134 is one of only two B[e]SGs showing broad emission from He II λ4686 [15]. The other object is LHA 115-S 18 in the SMC, which displays this (time variable) He II line in emission in concert with Raman-scattered O VI emission and TiO molecular emission features [40]. While for LHA 115-S 18, it was proposed that the peculiar spectral characteristics might point towards an LBV-like status of the star [40], a possible Wolf-Rayet companion was postulated to explain the spectral features of LHA 120-S 134 [97]. Although a solid proof for a Wolf-Rayet companion is still missing, LHA 120-S 134 has appeared since then in the catalog of LMC Wolf-Rayet stars (WR 146).

The mid-IR spectrum of LHA 120-S 134, obtained with the *Spitzer Space Telescope*, shows intense 10 µm and weak 20 µm emission features of amorphous silicate dust, and a faint and wispy nebulosity around the IR bright star was found with the telescope's imaging facilities [93]. Follow-up optical imaging revealed that LHA 120-S 134 is located on the northeast rim of the superbubble of DEM L269 and on the western rim of the H II region SGS LMC-2 [98]. Therefore, it is unclear if and how much of the optical and IR nebulosity might be related to LHA 120-S 134 itself.

In the NIR regime, the first mention of CO first-overtone emission dates back to 1985, when the star was observed with low-resolution [29]. The next *K*-band spectrum was taken only 24 years later (see Table 5). The new spectrum had higher spectral resolution, but the CO bands appeared to be similar to the previous detection. Our new, high-resolution spectrum was acquired after another time gap of 8 years. Our modeling of the band spectrum revealed basically the same CO parameters (temperature and column density) as in 2009, with one addition, the projected rotational velocity. As for LHA 120-S 12, this velocity is comparable to the one that might be inferred from the [Ca II] lines [94], and we may conclude that also LHA 120-S 134 is surrounded by a stable, rotating ring of atomic and molecular gas.
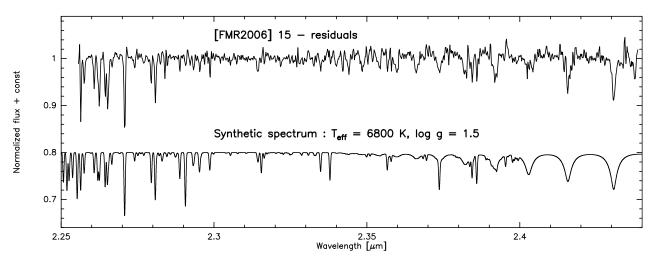
[FMR2006] 15 (=2MASS J18375778-0652320)

The star [FMR2006] 15 was recorded as object number 15 in a survey of the cool supergiant population of the massive young star cluster RSGC1 [88]. Based on the weak CO absorption detected in its *K*-band spectrum, a spectral type of G6 I was allocated. In a follow-up investigation, it was proposed that [FMR2006] 15 is most likely a YHG, based on the star's luminosity and spectral similarity to ρ Cas [71]. The star was assigned an effective temperature of 6850 ± 350 K and a luminosity of $\log L/L_\odot = 5.36^{+0.14}_{-0.16}$. With this temperature, the spectral type of [FMR2006] 15 is more likely G0 (± 2 subtypes), and the luminosity implies that the star lies with about $M_{\rm ini} \sim 25\,M_\odot$ in the lower mass range of stars developing into YHGs (see Figure 1). This relatively low initial mass was considered to be the reason for the lack of detectable intense IR excess emission and of maser emission in contrast to the high-mass YHGs such as, e.g., IRC +10420 [71].

The first low-resolution *K*-band spectrum of [FMR2006] 15 was taken in September 2005. At that time, very weak CO band absorption was seen [88]. Soon thereafter, the object was re-observed twice with considerably higher spectral resolution. In May 2006, the spectrum displayed CO band emission and in August 2006, the emission had disappeared [71]. Our detection of intense CO band emission 13 years later is a clear in-

dication that [FMR2006] 15 is embedded in circumstellar matter, even if the molecular gas is with 3000 K much too hot for the condensation of dust grains. When modeling the CO bands from [FMR2006] 15, we noticed that the CO emission displays a blue-shift of $-77\,\mathrm{km\,s^{-1}}$ with respect to the atmospheric absorption line spectrum. A similar behavior has been seen in IRC +10420. This star displays blue-shifted emission in its IR hydrogen recombination lines [99] and in its CO rotational transitions [45], which has been interpreted as emission formed in a close to pole-on seen bipolar outflow with the central star eclipsing the receding part of the emission. The outflow velocity from IRC +10420 has been measured to be on the order of $\sim 40\,\mathrm{km\,s^{-1}}$, which is about half the value we measure for [FMR2006] 15. To date, nothing is known about a possible orientation of [FMR2006] 15, but we might speculate that a similar scenario as for IRC +10420 might hold for that object as well. In such a case, we would expect to have a Gaussian-like distribution of the velocity (see bottom model in Figure 4).

On the other hand, if we consider the contribution from the rotation as real, the blue-shifted CO gas might revolve around a hidden companion, as in the case of the YHG HD 269953 in the LMC [51]. In this object, the companion was proposed to be surrounded by a gaseous disk traced by numerous emission lines that display a time-variable radial velocity offset with respect to the photospheric lines of the YHG star. If [FMR2006] 15 is indeed a binary system, time-resolved K-band observations would be essential to derive the orbital parameters and to characterize the hidden companion.

The best-fitting CO model has been subtracted from the *K*-band spectrum of [FMR2006] 15, and the residual is shown in Figure 5. Also included in this plot is a synthetic spectrum of a cool supergiant star with $T_{\mathrm{eff}} = 6800\,\mathrm{K}$ and $\log g = 1.5$, similar to the values derived for [FMR2006] 15 [71]. This spectrum has been computed with the spectrum synthesis code Turbospectrum using MARCS atmospheric models [100]. We note that the main photospheric features are decently well represented by this model. The short wavelength coverage of our spectrum and a possible alteration of the intrinsic stellar spectrum caused by the absorbing circumstellar gas impede a more decent classification of the object.

Figure 5. Residual spectrum of [FMR2006] 15 after subtraction of the blue-shifted CO band emission. For illustration purposes, a synthetic model spectrum of a cool supergiant is shown as well (shifted down along the flux axis for better visualization) with parameters similar to those determined for [FMR2006] 15.

6 Cas (=V566 Cas, HR 9018, HD 223385)

The object 6 Cas was reported to be a spectroscopic binary based on its composite spectrum in the ultraviolet [101]. While the main component is traced by the resonance lines of low-ionized metals with terminal wind velocities of about $330\,\mathrm{km\,s^{-1}}$, typical for A-type supergiants, the high-ionized resonance lines with P Cygni profiles and terminal wind velocities of about $2400\,\mathrm{km\,s^{-1}}$ can be assigned to a significantly hotter O-type companion.

Disentangling the spectra in the optical, to which the O star only very weakly contributes, resulted in the classification of the system as a A3 Ia (A) and a O9.5 II (B) component [79]. The positions of the two stars are separated by about 1″5 at a position angle of ∼195°. Whether these two stars form indeed a bound binary system or whether they are just close in projection could not be solved yet. The small radial velocity variations detected for the A supergiant seem to be due to pulsations rather than orbital motion in a binary system [79].

The Hα profile of 6 Cas resembles those seen in other hypergiants, such as HD 33579 and Schulte 12. It is superimposed on broad electron scattering wings [102]. Discrete absorption components (DACs) traveling through the broad absorption components of the wind profiles of H and Fe II lines were detected in 6 Cas [103]. Based on the atypical characteristics of a regular A-type supergiant, the star was assigned the status of a hypergiant.

We are aware of only one former *K*-band spectrum of 6 Cas, which has been taken with the ISO-SWS instrument [89]. This spectrum shows no indication of CO bands, just the lines of the Pfund series in absorption, similar to our spectrum (Figure 3). Such an otherwise featureless spectrum is consistent with a hot ($T_{\mathrm{eff}} > 8000\,\mathrm{K}$) star, in agreement with its previous classification (see Table 1).

V509 Cas (=HR 8752, HD 217476)

The star V509 Cas is one of the YHGs for which an outburst was recorded based on combined photometric and spectroscopic monitoring of the star [62]. This outburst must have taken place around 1973, after a preceding 16-year-long period of reddening and cooling of the object from about 5000 K down to about 4000 K [104]. Thereafter, the effective temperature of the star gradually increased until it reached a value of about 8000 K around 2001 [62], where it has stabilized since then [63]. During the "heating" period, several short-term drops in temperature were recorded, which were associated with phases of enhanced mass loss [62].

Despite the outburst and the multiple mass-loss events, no extended nebulosity was detected at optical wavelengths so far [66]. Nevertheless, the star must be embedded in an ionized circumstellar envelope traced by thermal emission at radio wavelengths [105,106]. The ionization of this envelope is most likely performed by the radiation field of a distant, hot main-sequence B1-type companion [107]. The envelope is also the place where other emission lines are formed. Most prominent are the nebular lines of [N II] $\lambda\lambda$ 6548,6583 [108], but also those of [O I] $\lambda\lambda$ 6300,6364 and [Ca II] $\lambda\lambda$ 7291,7324 were identified [63], which were proposed to trace a possible Keplerian disk or ring based on the double-peaked profiles, particularly of the [Ca II] lines, for which a rotation velocity, projected to the line of sight, of about $40\,\mathrm{km\,s^{-1}}$ was derived [109]. Support for such an interpretation comes from an optical spectroscopic monitoring of V509 Cas between 2015 and 2022. The observations revealed that the [Ca II] lines are stable in position and shape over the observing period of ∼7 years, in contrast to the photospheric absorption lines, whose shape and radial velocity are strongly influenced by the pulsation activity of the star [110].

In the NIR, observations dating back to 1979–1980 detected CO features displaying both emission and absorption components with variable strength (see Table 5, [70]). Comparison with the brightness curve revealed that the CO emission was strongest when the star was around maximum brightness [67]. Furthermore, the CO emission appeared at the stellar systemic velocity, whereas the absorption was either blue- or red-shifted. This behavior is very similar to what has been observed for the YHG star ρ Cas [67]. Since about 1988, the CO features have disappeared from the NIR spectra of V509 Cas, and our spectrum also shows no traces of molecular emission. The absorption lines of the hydrogen Pfund series seen in our otherwise featureless *K*-band spectrum are in agreement with a stellar temperature of about 8000 K.

HD 179821 (=RAFGL 2343, IRAS 19114+0002, V1427 Aql)

The star is embedded within a detached, almost spherical shell of cold (120–140 K) dust [49] responsible for an intense far-IR excess emission [111]. In the radio regime, CO ($J = 1 \longrightarrow 0$) emission has been detected, which traces a cold molecular outflow with a velocity of $\sim$33–35 km s^{-1} [112]. The object is oxygen-rich, as is inferred from its OH maser emission [113].

The evolutionary state of the star is highly debated in the literature due to its uncertain distance value. Distance estimates range from about 1.5 kpc to about 6 kpc, which would classify the star as either a post-asymptotic giant branch star or a YHG. Considering the newest parallax measurements of 0.1893 ± 0.0206 provided by the *GAIA* Early Data Release 3 [82], a distance closer to the upper value seems to be more likely. Such a high value is also in agreement with the star's kinematic distance derived from its large heliocentric systemic velocity of 84–88 km s^{-1} [81,112,113].

The spectral classification of HD 179821 has been rather controversial as well in the past decades ranging from F3–5 [81,114,115], over G5 [116] to K4 [117]. The value for $\log g$, derived from high-resolution spectroscopy, ranges around 0.5 ± 0.5. Such a low $\log g$ value assigns the star a luminosity class I.

Extinction values obtained for HD 179821 range from $A_V = 2.0$ [116] over 3.1 [118] to $\sim$4 [115], and it has been suggested that the total extinction might be variable due to possible changes in the circumstellar contribution from the dust shell [119].
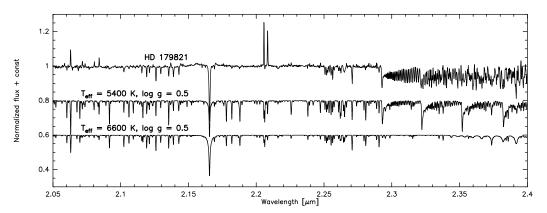
In a recent work, data from long-term photometric and spectroscopic monitoring have been presented [120]. The colors imply that the star first became bluer between 1990 and 1995 and has displayed a systematic reddening since 2002. The fastest change in color took place between 2013 and 2017, with a simultaneous brightening of the star. The spectra confirm this trend and record a more or less stable temperature of $T_{\text{eff}} = 6800 \pm 100$ K between 1994 and 2008, in agreement with previous temperature determinations [7] [81,114,115,120]. Since then, it decreased and reached a value of about 5900 K in 2017 [120]. The reddening and change in temperature indicate the onset of a possible new red loop evolution of HD 179821, i.e., an excursion to the cool edge of the HR diagram, related to a significant increase in the stellar radius and an increase in mass loss.

In the NIR, HD 179821 displayed CO-band emission, during observations taken between 1989 and 1991 (see Table 5), whereas no indication for CO band features (neither emission nor absorption) was seen between 1992 and 2000. The presence and disappearance of CO band emission might indicate a prior phase of higher mass loss or some mass ejection episode followed by the subsequent expansion and dilution of the released circumstellar material. Such a scenario might be supported by the redder color of the star around 1990 [120]. The absence of CO bands in the spectra between 1992 and 2000 supports the classification of the star as early to mid F-type, because stars in this temperature range are too hot for the formation of molecules in their atmospheres.

In contrast to all previous NIR observations, our data from 2021 clearly display CO band absorption. One possible explanation could be that the trend of cooling has continued since 2017. When comparing our observed spectra with synthetic spectra, we found that the intensity of the first band head of CO can be achieved for a stellar effective temperature of $\sim$5400 K (see Figure 6), although the entire CO band structure signals a considerably cooler temperature for the molecular gas due to the only weakly pronounced higher band heads. Hotter stars display less intense and cooler stars more intense CO bands. However, a star with a temperature of 5400 K should show significantly stronger absorption in all other atomic photospheric lines, which is not the case. Instead, the intensity and specific line ratios in the *K*-band spectrum are more in line with an effective temperature of about 6600 K. But such a hot stellar photosphere contains no CO molecular absorption features (Figure 6). Based on this discrepancy, we believe that our *K*-band spectrum is composite. It shows a hotter stellar photosphere along with CO absorption formed in a presumably cooler gas shell or outflow. Support for such a scenario is provided by the fact that the CO absorption bands display a

blue-shift of about $-43 \pm 1\,\mathrm{km\,s^{-1}}$ with respect to all other photospheric atomic lines and the circumstellar emission lines, such as the Na I doublet. If interpreted as outflow velocity, then this value is comparable to the outflow seen in IRC +10420 [45,99] but is slightly higher than the isotropic expanding cold molecular gas and dust shell around HD 179821 ($\sim 35\,\mathrm{km\,s^{-1}}$, [112,122]). We exclude a cool binary component as an explanation for the velocity-shifted CO absorption bands because, in this case, the cool companion would imprint (besides CO) significantly stronger blue-shifted absorption lines onto the *K*-band spectrum, which are not observed. If the proposed scenario of a new outflowing shell or gas layer is correct, possibly initiated during the reddening of the star and the increase in stellar radius recorded in the years 2014–2017 [120], or a possible outburst event that might have followed this reddening as in the case of V509 Cas (as we mentioned before, see [62,104]), then we may speculate that with further expansion of this matter, future *K*-band observations will display CO bands in emission before the material dilutes and the CO features might disappear again.

Besides CO, our spectrum of HD 179821 also shows Br γ in absorption and intense emission of the Na I doublet. The line of Br γ was in absorption in previous observations taken in 1989 [69] and 1990 [68]. The latter spectrum also displays intense emission of the (blended) Na I doublet, as well as the spectrum taken in 2000 [67]. The remaining previous spectra either do not cover the spectral region of Br γ and/or the Na I doublet, or these lines have not been mentioned by the corresponding authors.

Figure 6. Comparison of the *K*-band spectrum of HD 179821 (**top**) with synthetic spectra for effective temperatures of 5400 K (**middle**) and 6600 K (**bottom**). For illustration purposes, the synthetic model spectra are included in this figure and shifted down along the flux axis for better visualization.

Na I emission is a clear indicator for circumstellar material. It has been reported from the NIR spectra of numerous evolved massive stars: (i) the YHGs ρ Cas, V509 Cas, Hen 3-1379 (the Fried Egg Nebula), IRC +10420 [70,123], and the IRC +10420 analog IRAS 18357-0604 [124], (ii) most of the B[e]SGs [21,29,125], and (iii) also many luminous blue variables [21,53]. The equivalent widths of the intense Na I lines from the YHG IRC +10420 [6] are about three times higher than for HD 179821, for which we measured values of $-1.0670 \pm 0.015\,\text{Å}$ and $-0.9231 \pm 0.018\,\text{Å}$. Recent spatially resolved observations revealed that the Na I emission in IRC +10420 and Hen 3-1379 is confined within a compact spherical envelope around the star [50,123]. The emission lines in our spectrum are symmetric, and their wavelengths coincide with the systemic velocity of the star. While their formation region can be a compact spherical shell as well, they cannot be related to the possible new blue-shifted outflow traced by the CO band absorption.

5. Conclusions

We present new medium- and high-resolution *K*-band spectra for two B[e]SGs and four YHGs. The spectra of both B[e]SGs show rotationally broadened CO band emission, from which we could derive, for the first time, the projected rotation velocity of the CO gas for both stars. On the other hand, our model parameters for the CO temperature and

column density are very similar to those reported in previous studies based on spectra with significantly lower resolution [20,21]. The similarities of the detected CO band features over more than 30 years suggest that the CO emitting gas rings around these two B[e]SGs are stable structures, neatly fitting to the findings of most of the B[e]SGs.

With respect to the YHGs, we detect CO band emission from only one star, the highly reddened cluster member [FMR2006] 15, which previously showed time-variable CO features (see Table 5), and which has an effective temperature that is clearly too high to form molecules within its atmosphere. Consequently, the CO emission must be of circumstellar origin. A second object, HD 179821, shows CO bands in absorption, while it had CO emission during 1989–1991 but lacked any CO features in its spectrum since 1992 (Table 5). The latter is consistent with the star's high effective temperature, which prevents the formation of molecules. For both YHGs, our detected CO features are clearly blue-shifted with respect to the photospheric absorption lines, suggesting that both stars most likely had recent mass ejection events and the CO emission/absorption forms within the expelled matter. For [FMR2006] 15, we propose that the blue-shifted emission arises in a possible pole-on seen bipolar outflow as in the case of the YHG star IRC +10420 [6], but nothing can be said yet about the geometry of the outflow seen from HD 179821 because the (highly inflated) star itself might still block large portions of the possibly receding parts of the ejecta.

Abbreviations

The following abbreviations are used in this manuscript:

B[e]SG	B[e] supergiant
NIR	Near infrared
LMC	Large Magellanic Cloud
SMC	Small Magellanic Cloud
YHG	Yellow hypergiant

Notes

1.   The sixth object is LHA 120-S 111. To our knowledge, it has been observed in the *K*-band only once, in January 1987 [29]. At that time, no CO band emission was detected.

2.   We excluded two Galactic B[e]SGs from this plot. With a literature luminosity value of $\log L/L_\odot = 4.33 \pm 0.09$ [74], the luminosity of HD 62623 is considerably lower than for the other B[e]SGs with CO bands. However, its distance with a parallax value of 0.59 ± 0.17 is not well constrained. The object HD 327083 turned out to be misclassified and has been removed from the B[e]SGs list (Cidale et al., in preparation).

3.   We omit the SMC objects, because we do not have new data for any of the SMC B[e]SGs, and there are currently no confirmed YHGs in the SMC.

4.   IRAF is distributed by the National Optical Astronomy Observatory, which is operated by the Association of Universities for Research in Astronomy (AURA) under cooperative agreement with the National Science Foundation.

5.   Pfund line emission is also reported from LHA 120-S 12 [20], but in that star the maximum detected Pfund transition is with Pf(31) arising at 2.34 μm clearly outside our spectral coverage.

6.   https://www.unige.ch/sciences/astro/evolution/en/database/syclist/ (accessed on 1 April 2023).

7.   We note that a higher effective temperature of ~ 7350 K was proposed in the same period [121].

References

1. Brandner, W.; Grebel, E.K.; Chu, Y.H.; Weis, K. Ring Nebula and Bipolar Outflows Associated with the B1.5 Supergiant Sher 25 in NGC 3603. *Astrophys. J.* **1997**, *475*, L45–L48.
2. Hendry, M.A.; Smartt, S.J.; Skillman, E.D.; Evans, C.J.; Trundle, C.; Lennon, D.J.; Crowther, P.A.; Hunter, I. The blue supergiant Sher 25 and its intriguing hourglass nebula. *Mon. Not. R. Astron. Soc.* **2008**, *388*, 1127–1142.
3. Marston, A.P.; McCollum, B. Extended shells around B[e] stars. Implications for B[e] star evolution. *Astron. Astrophys.* **2008**, *477*, 193–202. [CrossRef]
4. Kraus, M.; Liimets, T.; Cappa, C.E.; Cidale, L.S.; Nickeler, D.H.; Duronea, N.U.; Arias, M.L.; Gunawan, D.S.; Oksala, M.E.; Fernandes, M.B.; et al. Resolving the Circumstellar Environment of the Galactic B[e] Supergiant Star MWC 137 from Large to Small Scales. *Astron. J.* **2017**, *154*, 186.
5. Smith, N.; Arnett, W.D.; Bally, J.; Ginsburg, A.; Filippenko, A.V. The ring nebula around the blue supergiant SBW1: Pre-explosion snapshot of an SN 1987A twin. *Mon. Not. R. Astron. Soc.* **2013**, *429*, 1324–1341.
6. Oudmaijer, R.D.; de Wit, W.J. Neutral and ionised gas around the post-red supergiant IRC +10 420 at AU size scales. *Astron. Astrophys.* **2013**, *551*, A69.
7. Lagadec, E.; Zijlstra, A.A.; Oudmaijer, R.D.; Verhoelst, T.; Cox, N.L.J.; Szczerba, R.; Mékarnia, D.; van Winckel, H. A double detached shell around a post-red supergiant: IRAS 17163-3907, the Fried Egg nebula. *Astron. Astrophys.* **2011**, *534*, L10.
8. Weis, K. Nebulae around Luminous Blue Variables-large bipolar variety. In *Active OB Stars: Structure, Evolution, Mass Loss, and Critical Limits*; Proceedings of the International Astronomical Union; Neiner, C., Wade, G., Meynet, G., Peters, G., Eds.; Cambridge University Press: Cambridge, UK, 2011; IAU Symposium No. 272, pp. 372–377. [CrossRef]
9. Liimets, T.; Kraus, M.; Moiseev, A.; Duronea, N.; Cidale, L.S.; Fariña, C. Follow-Up of Extended Shells around B[e] Stars. *Galaxies* **2022**, *10*, 41.
10. Chu, Y.H. Galactic ring nebulae associated with Wolf-rayet stars. I. Introduction and classification. *Astrophys. J.* **1981**, *249*, 195–200. [CrossRef]
11. Marston, A.P.; Chu, Y.H.; Garcia-Segura, G. A Survey of Nebulae around Galactic Wolf-Rayet Stars in the Southern Sky. I. *Astrophys. J. Suppl.* **1994**, *93*, 229. [CrossRef]
12. Marston, A.P.; Yocum, D.R.; Garcia-Segura, G.; Chu, Y.H. A Survey of Nebulae around Galactic Wolf-Rayet Stars in the Southern Sky. II. *Astrophys. J. Suppl.* **1994**, *95*, 151. [CrossRef]
13. Maryeva, O.V.; Koenigsberger, G.; Karpov, S.V.; Lozinskaya, T.A.; Egorov, O.V.; Rossi, C.; Calabresi, M.; Viotti, R.F. Asymmetrical nebula of the M33 variable GR290 (WR/LBV). *Astron. Astrophys.* **2020**, *635*, A201.
14. Sévigny, M.; St-Louis, N.; Drissen, L.; Martin, T. New insights into the WR nebula M1-67 with SITELLE. *Mon. Not. R. Astron. Soc.* **2021**, *501*, 5350–5361.

15. Zickgraf, F.J.; Wolf, B.; Stahl, O.; Leitherer, C.; Appenzeller, I. B(e)-supergiants of the Magellanic Clouds. *Astron. Astrophys.* **1986**, *163*, 119–134.

16. Domiciano de Souza, A.; Driebe, T.; Chesneau, O.; Hofmann, K.H.; Kraus, S.; Miroshnichenko, A.S.; Ohnaka, K.; Petrov, R.G.; Preisbisch, T.; Stee, P.; et al. AMBER/VLTI and MIDI/VLTI spectro-interferometric observations of the B[e] supergiant CPD-57°2874. Size and geometry of the circumstellar envelope in the near- and mid-IR. *Astron. Astrophys.* **2007**, *464*, 81–86. [CrossRef]

17. Maravelias, G.; Kraus, M.; Cidale, L.S.; Borges Fernandes, M.; Arias, M.L.; Curé, M.; Vasilopoulos, G. Resolving the kinematics of the discs around Galactic B[e] supergiants. *Mon. Not. R. Astron. Soc.* **2018**, *480*, 320–344.

18. Lamers, H.J.G.L.M.; Zickgraf, F.J.; de Winter, D.; Houziaux, L.; Zorec, J. An improved classification of B[e]-type stars. *Astron. Astrophys.* **1998**, *340*, 117–128.

19. Kraus, M. A Census of B[e] Supergiants. *Galaxies* **2019**, *7*, 83.

20. Liermann, A.; Kraus, M.; Schnurr, O.; Fernandes, M.B. The ^{13}Carbon footprint of B[e] supergiants. *Mon. Not. R. Astron. Soc.* **2010**, *408*, L6–L10.

21. Oksala, M.E.; Kraus, M.; Cidale, L.S.; Muratore, M.F.; Borges Fernandes, M. Probing the ejecta of evolved massive stars in transition. A VLT/SINFONI K-band survey. *Astron. Astrophys.* **2013**, *558*, A17.

22. Kraus, M. The pre-versus post-main sequence evolutionary phase of B[e] stars. Constraints from ^{13}CO band emission. *Astron. Astrophys.* **2009**, *494*, 253–262. .:200811020. [CrossRef]

23. Kraus, M.; Oksala, M.E.; Cidale, L.S.; Arias, M.L.; Torres, A.F.; Borges Fernandes, M. Discovery of SiO Band Emission from Galactic B[e] Supergiants. *Astrophys. J.* **2015**, *800*, L20.

24. Kraus, M.; Cidale, L.S.; Arias, M.L.; Maravelias, G.; Nickeler, D.H.; Torres, A.F.; Borges Fernandes, M.; Aret, A.; Curé, M.; Vallverdú, R.; et al. Inhomogeneous molecular ring around the B[e] supergiant LHA 120-S 73. *Astron. Astrophys.* **2016**, *593*, A112.

25. Kraus, M.; Oksala, M.E.; Nickeler, D.H.; Muratore, M.F.; Borges Fernandes, M.; Aret, A.; Cidale, L.S.; de Wit, W.J. Molecular emission from GG Carinae's circumbinary disk. *Astron. Astrophys.* **2013**, *549*, A28.

26. Muratore, M.F.; Kraus, M.; Oksala, M.E.; Arias, M.L.; Cidale, L.; Borges Fernandes, M.; Liermann, A. Evidence of the Evolved Nature of the B[e] Star MWC 137. *Astron. J.* **2015**, *149*, 13.

27. Torres, A.F.; Cidale, L.S.; Kraus, M.; Arias, M.L.; Barbá, R.H.; Maravelias, G.; Borges Fernandes, M. Resolving the clumpy circumstellar environment of the B[e] supergiant LHA 120-S 35. *Astron. Astrophys.* **2018**, *612*, A113.

28. Cidale, L.S.; Borges Fernandes, M.; Andruchow, I.; Arias, M.L.; Kraus, M.; Chesneau, O.; Kanaan, S.; Curé, M.; de Wit, W.J.; Muratore, M.F. Observational constraints for the circumstellar disk of the B[e] star CPD-52 9243. *Astron. Astrophys.* **2012**, *548*, A72. [CrossRef]

29. McGregor, P.J.; Hillier, D.J.; Hyland, A.R. CO Overtone Emission from Magellanic Cloud Supergiants. *Astrophys. J.* **1988**, *334*, 639. [CrossRef]

30. McGregor, P.J.; Hyland, A.R.; Hillier, D.J. Atomic and Molecular Line Emission from Early-Type High-Luminosity Stars. *Astrophys. J.* **1988**, *324*, 1071. [CrossRef]

31. Kraus, M.; Cidale, L.S.; Arias, M.L.; Oksala, M.E.; Borges Fernandes, M. Discovery of the First B[e] Supergiants in M 31. *Astrophys. J.* **2014**, *780*, L10.

32. Sholukhova, O.; Bizyaev, D.; Fabrika, S.; Sarkisyan, A.; Malanushenko, V.; Valeev, A. New luminous blue variables in the Andromeda galaxy. *Mon. Not. R. Astron. Soc.* **2015**, *447*, 2459–2467.

33. Oksala, M.E.; Kraus, M.; Arias, M.L.; Borges Fernandes, M.; Cidale, L.; Muratore, M.F.; Curé, M. The sudden appearance of CO emission in LHA 115-S 65. *Mon. Not. R. Astron. Soc.* **2012**, *426*, L56–L60.

34. Kraus, M.; Borges Fernandes, M.; de Araújo, F.X. Neutral material around the B[e] supergiant star LHA 115-S 65. An outflowing disk or a detached Keplerian rotating disk? *Astron. Astrophys.* **2010**, *517*, A30.

35. McGregor, P.J.; Hyland, A.R.; McGinn, M.T. Emission-line stars in the Magellanic Clouds: Infrared spectroscopy of Be and Ofpe/WN9 stars. *Astron. Astrophys.* **1989**, *223*, 237–240.

36. Morris, P.W.; Eenens, P.R.J.; Hanson, M.M.; Conti, P.S.; Blum, R.D. Infrared Spectra of Massive Stars in Transition: WNL, Of, Of/WN, Be, B[e], and Luminous Blue Variable Stars. *Astrophys. J.* **1996**, *470*, 597. [CrossRef]

37. Hamann, F.; Simon, M. Velocity-resolved Infrared Spectroscopy of MWC 349. *Astrophys. J.* **1986**, *311*, 909. [CrossRef]

38. Kraus, M.; Arias, M.L.; Cidale, L.S.; Torres, A.F. Evidence of an evolved nature of MWC 349A. *Mon. Not. R. Astron. Soc.* **2020**, *493*, 4308–4314.

39. Zickgraf, F.J.; Wolf, B.; Stahl, O.; Humphreys, R.M. S 18: A new B(e) supergiant in the Small Magellanic Cloud with evidence for an excretion disk. *Astron. Astrophys.* **1989**, *220*, 206–214.

40. Torres, A.F.; Kraus, M.; Cidale, L.S.; Barbá, R.; Borges Fernandes, M.; Brandi, E. Discovery of Raman-scattered lines in the massive luminous emission-line star LHA 115-S 18. *Mon. Not. R. Astron. Soc.* **2012**, *427*, L80–L84.

41. Oudmaijer, R.D.; Davies, B.; de Wit, W.J.; Patel, M. Post-Red Supergiants. In *Proceedings of the Biggest, Baddest, Coolest Stars: Proceedings of a Workshop Held at the Millennium Centre, Johnson City, TN, USA, 16–18 July 2007*; Astronomical Society of the Pacific Conference Series; Luttermoser, D.G., Smith, B.J., Stencel, R.E., Eds.; Astronomical Society of the Pacific: San Francisco, CA, USA, 2009; Volume 412, p. 17,

42. Ekström, S.; Georgy, C.; Eggenberger, P.; Meynet, G.; Mowlavi, N.; Wyttenbach, A.; Granada, A.; Decressin, T.; Hirschi, R.; Frischknecht, U.; et al. Grids of stellar models with rotation. I. Models from 0.8 to 120 M$_\odot$ at solar metallicity (Z = 0.014). *Astron. Astrophys.* **2012**, *537*, A146.

43. Smartt, S.J.; Eldridge, J.J.; Crockett, R.M.; Maund, J.R. The death of massive stars-I. Observational constraints on the progenitors of Type II-P supernovae. *Mon. Not. R. Astron. Soc.* **2009**, *395*, 1409–1437.

44. Smartt, S.J. Observational Constraints on the Progenitors of Core-Collapse Supernovae: The Case for Missing High-Mass Stars. *Publ. Astron. Soc. Aust.* **2015**, *32*, e016.

45. Oudmaijer, R.D.; Groenewegen, M.A.T.; Matthews, H.E.; Blommaert, J.A.D.L.; Sahu, K.C. The spectral energy distribution and mass-loss history of IRC + 10420. *Mon. Not. R. Astron. Soc.* **1996**, *280*, 1062–1070. [CrossRef]

46. Castro-Carrizo, A.; Lucas, R.; Bujarrabal, V.; Colomer, F.; Alcolea, J. SiO emission from a huge, detached shell in IRC + 10420. *Astron. Astrophys.* **2001**, *368*, L34–L37. [CrossRef]

47. Tiffany, C.; Humphreys, R.M.; Jones, T.J.; Davidson, K. The Morphology of IRC + 10420's Circumstellar Ejecta. *Astron. J.* **2010**, *140*, 339–349.

48. Deguchi, S.; Nakada, Y.; Sahai, R. SiO and CO emission from carbon stars with silicate features and southern IRAS sources. *Astron. Astrophys.* **1990**, *230*, 339–354.

49. Jura, M.; Werner, M.W. The Detached Dust Shell around the Massive Star HD 179821. *Astrophys. J.* **1999**, *525*, 113–L116. [CrossRef]

50. Koumpia, E.; Oudmaijer, R.D.; Graham, V.; Banyard, G.; Black, J.H.; Wichittanakom, C.; Ababakr, K.M.; de Wit, W.J.; Millour, F.; Lagadec, E.; et al. Optical and near-infrared observations of the Fried Egg Nebula. Multiple shell ejections on a 100 yr timescale from a massive yellow hypergiant. *Astron. Astrophys.* **2020**, *635*, A183.

51. Kourniotis, M.; Kraus, M.; Maryeva, O.; Borges Fernandes, M.; Maravelias, G. Revisiting the evolved hypergiants in the Magellanic Clouds. *Mon. Not. R. Astron. Soc.* **2022**, *511*, 4360–4376.

52. Humphreys, R.M.; Jones, T.J.; Polomski, E.; Koppelman, M.; Helton, A.; McQuinn, K.; Gehrz, R.D.; Woodward, C.E.; Wagner, R.M.; Gordon, K.; et al. M33's Variable A: A Hypergiant Star More Than 35 YEARS in Eruption. *Astron. J.* **2006**, *131*, 2105–2113.

53. Kourniotis, M.; Bonanos, A.Z.; Yuan, W.; Macri, L.M.; Garcia-Alvarez, D.; Lee, C.H. Monitoring luminous yellow massive stars in M 33: New yellow hypergiant candidates. *Astron. Astrophys.* **2017**, *601*, A76.

54. Nickeler, D.H.; Karlický, M. On the validity of ideal MHD in the vicinity of stagnation points in the heliosphere and other astrospheres. *Astrophys. Space Sci. Trans.* **2008**, *4*, 7–12. [CrossRef]

55. Glatzel, W. On the origin of strange modes and the mechanism of related instabilities. *Mon. Not. R. Astron. Soc.* **1994**, *271*, 66. [CrossRef]

56. Glatzel, W.; Kiriakidis, M.; Chernigovskij, S.; Fricke, K.J. The non-linear evolution of strange-mode instabilities. *Mon. Not. R. Astron. Soc.* **1999**, *303*, 116–124. [CrossRef]

57. Kraus, M.; Cidale, L.S.; Arias, M.L.; Torres, A.F.; Kolka, I.; Maravelias, G.; Nickeler, D.H.; Glatzel, W.; Liimets, T. Environments of evolved massive stars: Evidence for episodic mass ejections. *IAU Symp.* **2022**, *366*, 51–56. [CrossRef]

58. Lobel, A.; Dupree, A.K.; Stefanik, R.P.; Torres, G.; Israelian, G.; Morrison, N.; de Jager, C.; Nieuwenhuijzen, H.; Ilyin, I.; Musaev, F. High-Resolution Spectroscopy of the Yellow Hypergiant ρ Cassiopeiae from 1993 through the Outburst of 2000–2001. *Astrophys. J.* **2003**, *583*, 923–954.

59. Klochkova, V.G.; Panchuk, V.E.; Tavolzhanskaya, N.S. Changes of the Optical Spectrum of the Hypergiant ρ Cas due to a Shell Ejection in 2013. *Astron. Rep.* **2018**, *62*, 623–635.

60. Kraus, M.; Kolka, I.; Aret, A.; Nickeler, D.H.; Maravelias, G.; Eenmäe, T.; Lobel, A.; Klochkova, V.G. A new outburst of the yellow hypergiant star ρ Cas. *Mon. Not. R. Astron. Soc.* **2019**, *483*, 3792–3809.

61. Maravelias, G.; Kraus, M. Bouncing against the Yellow Void-Exploring the Outbursts of rho Cassiopeiae from Visual Observations. *J. Am. Assoc. Variable Star Observers* **2022**, *50*, 49.

62. Nieuwenhuijzen, H.; De Jager, C.; Kolka, I.; Israelian, G.; Lobel, A.; Zsoldos, E.; Maeder, A.; Meynet, G. The hypergiant HR 8752 evolving through the yellow evolutionary void. *Astron. Astrophys.* **2012**, *546*, A105. [CrossRef]

63. Aret, A.; Kolka, I.; Kraus, M.; Maravelias, G. Similarities in the Structure of the Circumstellar Environments of B[e] Supergiants and Yellow Hypergiants. In *Proceedings of the The B[e] Phenomenon: Forty Years of Studies, Prague, Czech Republic, 27 June–1 July 2016*; Astronomical Society of the Pacific Conference Series; Miroshnichenko, A., Zharikov, S., Korčáková, D., Wolf, M., Eds.; Astronomical Society of the Pacific: San Francisco, CA, USA, 2017; Volume 508, p. 239,

64. Oudmaijer, R.D. High resolution spectroscopy of the post-red supergiant IRC+10420. I. The data. *Astron. Astrophys. Suppl. Ser.* **1998**, *129*, 541–552. .:1998404. [CrossRef]

65. Klochkova, V.G.; Yushkin, M.V.; Chentsov, E.L.; Panchuk, V.E. Evolutionary Changes in the Optical Spectrum of the Peculiar Supergiant IRC + 10420. *Astron. Rep.* **2002**, *46*, 139–151. [CrossRef]

66. Schuster, M.T.; Humphreys, R.M.; Marengo, M. The Circumstellar Environments of NML Cygni and the Cool Hypergiants. *Astron. J.* **2006**, *131*, 603–611.

67. Gorlova, N.; Lobel, A.; Burgasser, A.J.; Rieke, G.H.; Ilyin, I.; Stauffer, J.R. On the CO Near-Infrared Band and the Line-splitting Phenomenon in the Yellow Hypergiant ρ Cassiopeiae. *Astrophys. J.* **2006**, *651*, 1130–1150.

68. Hrivnak, B.J.; Kwok, S.; Geballe, T.R. Near-Infrared Spectroscopy of Proto–Planetary Nebulae. *Astrophys. J.* **1994**, *420*, 783. [CrossRef]

69. Oudmaijer, R.D.; Waters, L.B.F.M.; van der Veen, W.E.C.J.; Geballe, T.R. Near-infrared spectroscopy of post-AGB stars. *Astron. Astrophys.* **1995**, *299*, 69.

70. Lambert, D.L.; Hinkle, K.H.; Hall, D.N.B. Circumstellar shells of luminous supergiants. I. Carbon monoxide in rho CAS and HR 8752. *Astrophys. J.* **1981**, *248*, 638–650. [CrossRef]

71. Davies, B.; Figer, D.F.; Law, C.J.; Kudritzki, R.P.; Najarro, F.; Herrero, A.; MacKenty, J.W. The Cool Supergiant Population of the Massive Young Star Cluster RSGC1. *Astrophys. J.* **2008**, *676*, 1016–1028.

72. Kraus, M.; Arias, M.L.; Cidale, L.S.; Torres, A.F.; Kourniotis, M. Molecular environment of the yellow hypergiant star HD 269953. *Bol. Asoc. Argent. Astron. Plata Argent.* **2022**, *63*, 65–67.

73. Muratore, M.F.; Kraus, M.; de Wit, W.J. Near-infrared spectroscopic survey of galactic B[e] stars. *Bol. Asoc. Argent. Astron. Plata Argent.* **2012**, *55*, 123–127.

74. Millour, F.; Meilland, A.; Chesneau, O.; Stee, P.; Kanaan, S.; Petrov, R.; Mourard, D.; Kraus, S. Imaging the spinning gas and dust in the disc around the supergiant A[e] star HD 62623. *Astron. Astrophys.* **2011**, *526*, A107.

75. de Jager, C. The yellow hypergiants. *Astron. Astrophys. Rev.* **1998**, *8*, 145–180. [CrossRef]

76. Eggenberger, P.; Ekström, S.; Georgy, C.; Martinet, S.; Pezzotti, C.; Nandal, D.; Meynet, G.; Buldgen, G.; Salmon, S.; Haemmerlé, L.; et al. Grids of stellar models with rotation. VI. Models from 0.8 to 120 M$_\odot$ at a metallicity Z = 0.006. *Astron. Astrophys.* **2021**, *652*, A137.

77. Pietrzyński, G.; Graczyk, D.; Gallenne, A.; Gieren, W.; Thompson, I.B.; Pilecki, B.; Karczmarek, P.; Górski, M.; Suchomska, K.; Taormina, M.; et al. A distance to the Large Magellanic Cloud that is precise to one per cent. *Nature* **2019**, *567*, 200–203.

78. Kudritzki, R.P.; Puls, J.; Lennon, D.J.; Venn, K.A.; Reetz, J.; Najarro, F.; McCarthy, J.K.; Herrero, A. The wind momentum-luminosity relationship of galactic A- and B-supergiants. *Astron. Astrophys.* **1999**, *350*, 970–984.

79. Maíz Apellániz, J.; Barbá, R.H.; Fariña, C.; Sota, A.; Pantaleoni González, M.; Holgado, G.; Negueruela, I.; Simón-Díaz, S. Lucky spectroscopy, an equivalent technique to lucky imaging. II. Spatially resolved intermediate-resolution blue-violet spectroscopy of 19 close massive binaries using the William Herschel Telescope. *Astron. Astrophys.* **2021**, *646*, A11.

80. de Jager, C.; Nieuwenhuijzen, H. An obstacle to the late evolution of massive stars. *Mon. Not. R. Astron. Soc.* **1997**, *290*, L50–L54. [CrossRef]

81. Kipper, T. Optical Spectroscopy of a Post-Agb Star HD 179821 (V1427 Aql). *Balt. Astron.* **2008**, *17*, 87–102.

82. Gaia Collaboration. VizieR Online Data Catalog: Gaia EDR3 (Gaia Collaboration, 2020). *VizieR Online Data Catalog* **2020**, I/350. [CrossRef]

83. Cutri, R.M.; Skrutskie, M.F.; van Dyk, S.; Beichman, C.A.; Carpenter, J.M.; Chester, T.; Cambresy, L.; Evans, T.; Fowler, J.; Gizis, J.; et al. VizieR Online Data Catalog: 2MASS All-Sky Catalog of Point Sources (Cutri + 2003). *VizieR Online Data Catalog* **2003**, II/246.

84. Hinkle, K.H.; Blum, R.D.; Joyce, R.R.; Sharp, N.; Ridgway, S.T.; Bouchet, P.; van der Bliek, N.S.; Najita, J.; Winge, C. The Phoenix Spectrograph at Gemini South. In *Discoveries and Research Prospects from 6- to 10-Meter-Class Telescopes II*; Guhathakurta, P., Ed.; Society of Photo-Optical Instrumentation Engineers (SPIE) Conference Series; 2003; Volume 4834, pp. 353–363. [CrossRef]

85. Elias, J.H.; Rodgers, B.; Joyce, R.R.; Lazo, M.; Doppmann, G.; Winge, C.; Rodríguez-Ardila, A. Performance of the Gemini near-infrared spectrograph. In *Proceedings of the Society of Photo-Optical Instrumentation Engineers (SPIE) Conference Series*; McLean, I.S., Iye, M., Eds.; Society of Photo-Optical Instrumentation Engineers (SPIE): Bellingham, WA, USA, 2006; Volume 6269, p. 626914. [CrossRef]

86. Elias, J.H.; Joyce, R.R.; Liang, M.; Muller, G.P.; Hileman, E.A.; George, J.R. Design of the Gemini near-infrared spectrograph. In *Proceedings of the Society of Photo-Optical Instrumentation Engineers (SPIE) Conference Series*; McLean, I.S., Iye, M., Eds.; Society of Photo-Optical Instrumentation Engineers (SPIE): Bellingham, WA, USA, 2006; Volume 6269, p. 62694C. [CrossRef]

87. Kraus, M.; Krügel, E.; Thum, C.; Geballe, T.R. CO band emission from MWC 349. I. First overtone bands from a disk or from a wind? *Astron. Astrophys.* **2000**, *362*, 158–168.

88. Figer, D.F.; MacKenty, J.W.; Robberto, M.; Smith, K.; Najarro, F.; Kudritzki, R.P.; Herrero, A. Discovery of an Extraordinarily Massive Cluster of Red Supergiants. *Astrophys. J.* **2006**, *643*, 1166–1179.

89. Vandenbussche, B.; Beintema, D.; de Graauw, T.; Decin, L.; Feuchtgruber, H.; Heras, A.; Kester, D.; Lahuis, F.; Lenorzer, A.; Lorente, R.; et al. The ISO-SWS post-helium atlas of near-infrared stellar spectra. *Astron. Astrophys.* **2002**, *390*, 1033–1048. [CrossRef]

90. Henize, K.G. Catalogues of Hα-emission Stars and Nebulae in the Magellanic Clouds. *Astrophys. J. Suppl.* **1956**, *2*, 315. [CrossRef]

91. Stahl, O.; Leitherer, C.; Wolf, B.; Zickgraf, F.J. Three new hot stars with dust shells in the Magellanic clouds. *Astron. Astrophys.* **1984**, *131*, L5–L6.

92. Magalhaes, A.M. Polarization and the Envelopes of B[e] Supergiants in the Magellanic Clouds. *Astrophys. J.* **1992**, *398*, 286. [CrossRef]

93. Kastner, J.H.; Buchanan, C.; Sahai, R.; Forrest, W.J.; Sargent, B.A. The Dusty Circumstellar Disks of B[e] Supergiants in the Magellanic Clouds. *Astron. J.* **2010**, *139*, 1993–2002. [CrossRef]

94.   Aret, A.; Kraus, M.; Muratore, M.F.; Borges Fernandes, M. A new observational tracer for high-density disc-like structures around B[e] supergiants. *Mon. Not. R. Astron. Soc.* **2012**, *423*, 284–293.

95.   Merrill, P.W.; Burwell, C.G. Catalogue and Bibliography of Stars of Classes B and A whose Spectra have Bright Hydrogen Lines. *Astrophys. J.* **1933**, *78*, 87. [CrossRef]

96.   Shore, S.N.; Sanduleak, N. The extreme LMC supergiant HD 38489: An optical and ultraviolet study. *Astrophys. J.* **1983**, *273*, 177–186. [CrossRef]

97.   Massey, P.; Neugent, K.F.; Morrell, N.; Hillier, D.J. A Modern Search for Wolf-Rayet Stars in the Magellanic Clouds: First Results. *Astrophys. J.* **2014**, *788*, 83.

98.   Hung, C.S.; Ou, P.S.; Chu, Y.H.; Gruendl, R.A.; Li, C.J. A Multiwavelength Survey of Wolf-Rayet Nebulae in the Large Magellanic Cloud. *Astrophys. J. Suppl.* **2021**, *252*, 21.

99.   Oudmaijer, R.D.; Geballe, T.R.; Waters, L.B.F.M.; Sahu, K.C. Discovery of near-infrared hydrogen line emission in the peculiar F8 hypergiant IRC + 10420. *Astron. Astrophys.* **1994**, *281*, L33–L36.

100.   Plez, B. *Turbospectrum: Code for Spectral Synthesis*; record ascl:1205.004; ASCL.net, Michigan Technological University: Houghton, MI, USA, 2012.

101.   Talavera, A.; Gomez de Castro, A.I. The UV high resolution spectrum of A-type supergiants. *Astron. Astrophys.* **1987**, *181*, 300–314.

102.   Klochkova, V.G.; Chentsov, E.L. The Problem of Spectral Mimicry of Supergiants. *Astron. Rep.* **2018**, *62*, 19–30.

103.   Chentsov, E.L. Unstable Wind of 6 Cassiopeiae. *Astrophys. Space Sci.* **1995**, *232*, 217–232. [CrossRef]

104.   Luck, R.E. An analysis of the superluminous star HR 8752. *Astrophys. J.* **1975**, *202*, 743–754. [CrossRef]

105.   Smolinski, J.; Feldman, P.A.; Higgs, L.A. A search for radio emission from late-type supergiant stars. *Astron. Astrophys.* **1977**, *60*, 277–280.

106.   Higgs, L.A.; Feldman, P.A.; Smolinski, J. The radio source associated with the G-type supergiant HR 8752. *Astrophys. J.* **1978**, *220*, L109–L112. [CrossRef]

107.   Stickland, D.J.; Harmer, D.L. The discovery of a hot companion to HR 8752. *Astron. Astrophys.* **1978**, *70*, L53–L56.

108.   Sargent, W.L.W. Forbidden emission lines in the spectrum of a G-type supergiant. *Observatory* **1965**, *85*, 33–35.

109.   Aret, A.; Kraus, M.; Kolka, I.; Maravelias, G. The Yellow Hypergiant-B[e] Supergiant Connection. In *Proceedings of the Stars: From Collapse to Collapse, Nizhny Arkhyz, Russia, 3–7 October 2016*; Astronomical Society of the Pacific Conference Series; Balega, Y.Y., Kudryavtsev, D.O., Romanyuk, I.I., Yakunin, I.A., Eds.; Astronomical Society of the Pacific: San Francisco, CA, USA, 2017; Volume 510, p. 162,

110.   Kasikov, A.; Kolka, I.; Aret, A. Following V509 Cas into the void with FIES. In *Proceedings of the NOT—A Telescope for the Future, La Palma, Canary Islands, Spain, 7–10 June 2022*; CERN: Geneva, Switzerland, 2022; p. 14. [CrossRef]

111.   van der Veen, W.E.C.J.; Habing, H.J.; Geballe, T.R. Objects in transition from the AGB to the planetary nebula stage: New visual and infrared observations. *Astron. Astrophys.* **1989**, *226*, 108–136.

112.   Zuckerman, B.; Dyck, H.M. Dust Grains and Gas in the Circumstellar Envelopes around Luminous Red-Giant Stars. *Astrophys. J.* **1986**, *311*, 345. [CrossRef]

113.   Likkel, L. OH and H_2O Observations of Cold IRAS Stars. *Astrophys. J.* **1989**, *344*, 350. [CrossRef]

114.   Zacs, L.; Klochkova, V.G.; Panchuk, V.E.; Spelmanis, R. The chemical composition of the protoplanetary nebula candidate HD 179821. *Mon. Not. R. Astron. Soc.* **1996**, *282*, 1171–1180. [CrossRef]

115.   Reddy, B.E.; Hrivnak, B.J. Spectroscopic Study of HD 179821 (IRAS 19114 + 0002): Proto-Planetary Nebula or Supergiant? *Astron. J.* **1999**, *117*, 1834–1844. [CrossRef]

116.   Hrivnak, B.J.; Kwok, S.; Volk, K.M. A Study of Several F and G Supergiant-like Stars with Infrared Excesses as Candidates for Proto–Planetary Nebulae. *Astrophys. J.* **1989**, *346*, 265. [CrossRef]

117.   Odenwald, S.F. An IRAS Survey of Infrared Excesses in G-Type Stars. *Astrophys. J.* **1986**, *307*, 711. [CrossRef]

118.   Arkhipova, V.P.; Ikonnikova, N.P.; Noskova, R.I.; Sokol, G.V.; Shugarov, S.Y. Light Variations in the Candidate for Protoplanetary Objects HD 179821 = V1427 Aql in 1899–1999. *Astron. Lett.* **2001**, *27*, 156–162. [CrossRef]

119.   Arkhipova, V.P.; Esipov, V.F.; Ikonnikova, N.P.; Komissarova, G.V.; Tatarnikov, A.M.; Yudin, B.F. Photometric variability and evolutionary status of the supergiant with an infrared excess HD 179821 = V1427 aquilae. *Astron. Lett.* **2009**, *35*, 764–779. [CrossRef]

120.   Ikonnikova, N.P.; Taranova, O.G.; Arkhipova, V.P.; Komissarova, G.V.; Shenavrin, V.I.; Esipov, V.F.; Burlak, M.A.; Metlov, V.G. Multicolor Photometry and Spectroscopy of the Yellow Supergiant with Dust Envelope HD 179821 = V1427 Aquilae. *Astron. Lett.* **2018**, *44*, 457–473.

121.   Şahin, T.; Lambert, D.L.; Klochkova, V.G.; Panchuk, V.E. HD 179821 (V1427 Aql, IRAS 19114 + 0002)—A massive post-red supergiant star? *Mon. Not. R. Astron. Soc.* **2016**, *461*, 4071–4087.

122.   Castro-Carrizo, A.; Quintana-Lacaci, G.; Bujarrabal, V.; Neri, R.; Alcolea, J. Arcsecond-resolution ^{12}CO mapping of the yellow hypergiants IRC + 10420 and AFGL 2343. *Astron. Astrophys.* **2007**, *465*, 457–467. [CrossRef]

123.   Koumpia, E.; Oudmaijer, R.D.; de Wit, W.J.; Mérand, A.; Black, J.H.; Ababakr, K.M. Tracing a decade of activity towards a yellow hypergiant. The spectral and spatial morphology of IRC + 10420 at au scales. *Mon. Not. R. Astron. Soc.* **2022**, *515*, 2766–2777.

124. Clark, J.S.; Negueruela, I.; González-Fernández, C. IRAS 18357-0604—An analogue of the galactic yellow hypergiant IRC + 10420? *Astron. Astrophys.* **2014**, *561*, A15.

125. Arias, M.L.; Vallverdú, R.; Torres, A.F.; Kraus, M. *High-Resolution, Near-Infrared Observations of B[e] Supergiants*; Boletin de la Asociacion Argentina de Astronomia: La Plata, Argentina, 2021; Volume 62, pp. 104–106.